THE ASTROPHYSICAL JOURNAL, 492:428–438, 1998 January 10

A LARGE STRUCTURE OF GALAXIES AT REDSHIFT $z \sim 3$ AND ITS COSMOLOGICAL IMPLICATIONS[1]

CHARLES C. STEIDEL[2,3] AND KURT L. ADELBERGER
Palomar Observatory, Caltech 105-24, Pasadena, CA 91125
MARK DICKINSON[4,5]
Department of Physics and Astronomy, The Johns Hopkins University, Baltimore, MD 21218
MAURO GIAVALISCO[6]
The Carnegie Observatories, 813 Santa Barbara Street, Pasadena, CA 91101
MAX PETTINI
Royal Greenwich Observatory, Madingley Road, Cambridge CB3 0EZ, UK
AND
MELINDA KELLOGG
Palomar Observatory, Caltech 105-24, Pasadena, CA 91125
Received 1997 June 27; accepted 1997 August 18

ABSTRACT

We report the discovery of a highly significant concentration of galaxies at a redshift of $\langle z \rangle = 3.090$. The structure is evident in a redshift histogram of photometrically selected "Lyman-break" objects in a 9′ by 18′ field in which we have obtained 78 spectroscopic redshifts in the range $2.0 \leq z \leq 3.4$. The dimensions of the structure projected on the plane of the sky are at least 11′ by 8′, or 14 h_{70}^{-1} by 10 h_{70}^{-1} Mpc (comoving; $\Omega_M = 1$). The concentration contains 15 galaxies and one faint ($\mathscr{R} = 21.7$) QSO. We consider the structure in the context of a number of cosmological models and argue that Lyman-break galaxies must be very biased tracers of mass, with an effective bias on mass scale $M \sim 10^{15}\ M_\odot$ ranging from $b \sim 2$ for $\Omega_M = 0.2$ to $b \gtrsim 6$ for $\Omega_M = 1$. In a cold dark matter scenario, the large bias values suggest that individual Lyman-break galaxies are associated with dark halos of mass $M \sim 10^{12}\ M_\odot$, reinforcing the interpretation of these objects as the progenitors of massive galaxies at the present epoch. Preliminary results of spectroscopy in additional fields suggest that such large structures are common at $z \sim 3$, with about one similar structure per survey field. The implied space density is consistent with the possibility that we are observing moderately rich clusters of galaxies in their early nonlinear evolution. Finally, the spectrum of one of the QSOs discovered in our survey ($z_{\rm em} = 3.356$) exhibits metal-line absorption systems within the three redshift bins having the largest number of galaxies in field, $z = 2.93$, 3.09, and 3.28. These results are the first from an ongoing "targeted" redshift survey designed to explore the nature and distribution of star-forming galaxies in the redshift range $2.7 \lesssim z \lesssim 3.4$.

Subject headings: galaxies: distances and redshifts — galaxies: evolution — galaxies: formation — large-scale structure of universe

1. INTRODUCTION

The large-scale distribution of galaxies at early epochs provides a powerful means of discriminating among various cosmological world models and mechanisms for the formation of structure (see, e.g., White 1997, and references therein). The most comprehensive surveys of the large-scale distribution of galaxies have been carried out in the relatively "local" universe (see, e.g., Shectman et al. 1996), while hints of what is happening at larger redshifts ($z \lesssim 0.8$) have been obtained using pencil-beam apparent-magnitude–limited redshift surveys (see, e.g., Broadhurst et al. 1990; Carlberg et al. 1997; Le Fèvre et al. 1996; Connolly et al. 1996; Cohen et al. 1996a, 1996b). A general result seems to be that the (small-scale) correlation function of the more distant galaxies is reduced significantly in amplitude relative to the present time (see, e.g., Efstathiou 1995; Brainerd, Smail, & Mould 1995; Le Févre et al. 1996), while on larger scales the one-dimensional "line-of-sight" structures appear to be quite prominent to at least $z \sim 1$, with a typical comoving distance between structures of $\sim 100\ h^{-1}$ Mpc along the line of sight. It is not yet clear how these two observational results should be combined to form a coherent picture since it is so difficult to obtain information in the "transverse" direction in surveys of faint galaxies, so the nature of the structures giving rise to the "spikes" in one-dimensional redshift surveys is ambiguous (Kaiser & Peacock 1991). Locally, at least, it appears that the line-of-sight structures seen in the pencil-beam surveys are likely to be related to the cell-like "wall-void" geometry seen in more extensive, large solid-angle redshift surveys (see, e.g., de Lapparent, Geller, & Huchra 1986; Landy et al. 1996).

In addition to the difficulties presented by the "geometry" of very deep redshift surveys, it is not clear to what extent galaxies are reliable tracers of mass, particularly at high redshifts where a large degree of "bias" is expected for objects forming within massive dark matter halos (see, e.g., Bardeen et al. 1986; Brainerd & Villumsen 1992; Mo & Fukugita 1996; Baugh et al. 1998). However, a measurement of the bias of a class of objects at high redshift

[1] Based in part on observations obtained at the W. M. Keck Observatory, which is operated jointly by the California Institute of Technology and the University of California.
[2] Alfred P. Sloan Foundation Fellow.
[3] NSF Young Investigator.
[4] Alan C. Davis Fellow.
[5] Also Space Telescope Science Institute.
[6] Hubble Fellow.

(and the evolution of the bias with redshift) can be used to constrain the connection between the sites of their formation and the overall mass distribution, which can in turn be used to constrain models of structure and galaxy formation (see, e.g., Cole & Kaiser 1989; Mo & White 1996).

In this paper, we present the first results of a large survey of the galaxy distribution at $z \sim 3$. Efficient photometric selection of star-forming objects at high redshift (Steidel, Pettini, & Hamilton 1995; Steidel et al. 1996a, 1996b) and subsequent spectroscopy on the W. M. Keck telescopes allow an assessment of the growth of structure in the galaxy distribution at significantly higher redshift than has been previously accessible. In a separate paper (Giavalisco et al. 1998), we analyze the angular correlation function of the photometrically selected $z \sim 3$ galaxy candidates in a number of fields. Here we focus on a single field in which we have obtained the most complete spectroscopic observations to date, with data analogous to "pencil-beam" surveys at smaller redshifts. Aside from probing the structures traced by galaxies at significantly earlier epochs than has been possible previously, working at $z \sim 3$ also has the advantage that a reasonable angular scale for multiobject spectroscopy on large telescopes maps onto relatively large comoving scales; our field size of 9′ by 18′ at $z \sim 3$ traces (transverse) structure equivalent to a field 24′ by 48′ at $z \sim 0.5$. As we will discuss below, the relatively large transverse comoving scale provides a distinct advantage in assessing the galaxy clustering properties on scales that remain in the linear regime to the present day, allowing for a relatively straightforward analytic treatment.

In this paper, we use the first observations of relatively large-scale structure traced by star-forming galaxies at $z \sim 3$ to estimate the amount by which this population must be biased relative to the overall mass distribution expected for standard cosmological models. The measurement of this bias will allow us to infer a corresponding dark matter halo mass scale and makes possible future direct comparisons with gravitational N-body and semianalytic simulations of early structure formation. We will show that the implied halo mass scale of the "Lyman-break galaxies" supports the conclusion that they likely represent the progenitors of the massive galaxies of the present epoch (Steidel et al. 1996b; Giavalisco, Steidel, & Machetto 1996; Mo & Fukugita 1996; Baugh et al. 1998).

2. OBSERVATIONS

The present work focuses on one of the fields in a survey of $z \sim 3$ galaxies based on ground-based images in the U_n, G, and $\mathcal{R}$ photometric system (Steidel & Hamilton 1993), which is designed to be sensitive to the Lyman break in objects having redshifts primarily in the range $2.7 \leq z \leq 3.4$. A complete description of the observations and techniques used in this survey will be published elsewhere (Steidel et al. 1998). The field under discussion consists of two adjacent pointings of the Palomar 5 m Hale telescope with the COSMIC prime focus camera. The camera uses a thinned, AR-coated Tektronix 2048 × 2048 CCD with a scale of 0.″283 pixel^{-1}. The images were obtained in 1995 August and 1996 August and typically reach 1 σ surface-brightness limits of 29 (AB) mag arcsec^{-2} in each passband. The northern field is centered on the "SSA 22" deep redshift survey field of Cowie et al. (1996), at $\alpha = 22^{\rm h}17^{\rm m}34^{\rm s}.0$, $\delta = +00°15'01''$ (J2000) and includes most of a nearby region observed as part of the Canada-France Redshift Survey (Lilly et al. 1995). The southern field is centered 525″ south of that position. The size of the full contiguous field is 17.′64 in the north-south direction and 8.′74 in the east-west direction. We refer to the two separate pointings as "SSA 22a" and "SSA 22b" for the northern and southern fields, respectively.

Spectroscopic observations of Lyman-break candidates were obtained using the Keck I telescope in 1995 October and 1996 August and using the Keck II telescope in its first week of scientific observations during 1996 October. We obtained spectra of as many candidates as possible by using seven different slit masks with the Low-Resolution Imaging Spectrograph (Oke et al. 1995), each covering roughly 4′ by 7′ regions and including ∼15–20 candidate objects per mask. Typical total exposure times were 1.5–3 hr per mask, in separate 1800 s integrations. The resolution of the spectra, using a 300 line mm^{-1} grating, was approximately 12 Å, and the grating tilt was adjusted so that the wavelength coverage for each slit included the 4300–7000 Å range. Objects were assigned slits based on a number of factors, the most important being the maximization of the number of $z \sim 3$ candidates on each mask. Objects were prioritized on the basis of how unambiguously the Lyman discontinuity could be discerned from the broadband photometry. About two-thirds of the objects discussed here satisfied our "robust" color criteria (see Steidel et al. 1995), $\mathcal{R} \leq 25.5$, $G - \mathcal{R} \leq 1.2$, and $U_n - G \geq G - \mathcal{R} + 1.5$, while the rest were selected using our "marginal" criteria, $\mathcal{R} \leq 25.5$, $G - \mathcal{R} \leq 1.2$, and $G - \mathcal{R} + 1.0 \leq U_n - G \leq G - \mathcal{R} + 1.5$. In practice, most of the marginal candidates that have been observed spectroscopically also have $U_n - G > 1.6$, in order to maximize the number of galaxies in

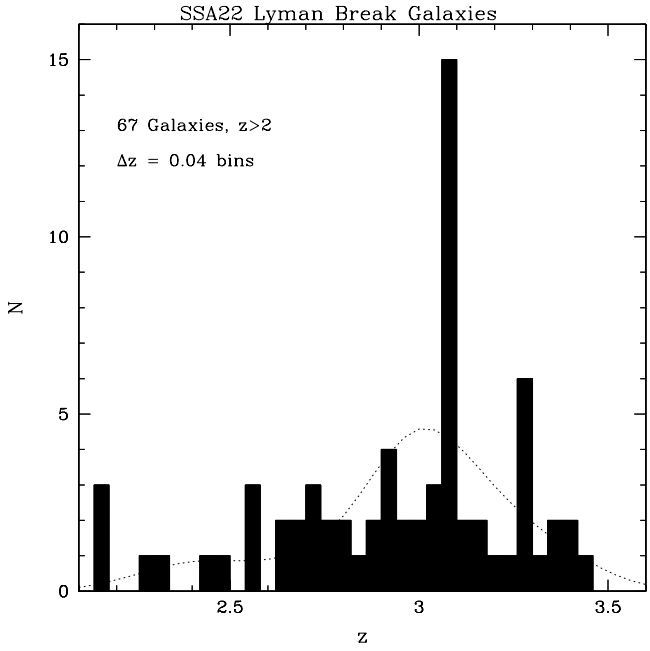

FIG. 1.—Redshift histogram of the 67 color-selected objects with $z > 2$ that have been confirmed spectroscopically in an 8.′7 by 17.′6 strip. The dotted curve represents the smoothed redshift selection function obtained to date for our overall survey, normalized so as to have the same number of total galaxies as the SSA 22 sample. Approximately one-third of the confirmed redshifts are from the SSA 22 fields. The binning here is arbitrary; the formal boundaries of any "features" in the redshift distribution used for analysis were obtained using the method described in § 3 and in the Appendix.

TABLE 1

OBJECTS WITHIN THE $\langle z \rangle = 3.09$ STRUCTURE

Object	R.A.[a] (arcmin)	Decl.[a] (arcmin)	$\mathscr{R}$	$G - \mathscr{R}$	$U_n - G$	Redshift[b]	Star Formation Rate[c]
SSA 22a C3	3.1	9.2	24.53	0.48	>2.48	3.074	12.3
SSA 22b C32	1.0	6.8	24.89	0.50	>2.32	3.074	8.7
SSA 22a C23.....	7.6	15.3	25.09	0.55	>2.17	3.075	7.3
SSA 22a C14.....	2.1	13.5	25.07	0.79	>2.33	3.081	7.4
SSA 22a D13	3.7	14.5	21.59	0.35	2.28	3.083	QSO
SSA 22b D27	7.3	6.2	25.13	0.29	2.18	3.086	7.1
SSA 22a D2.....	4.8	9.7	23.39	0.95	2.61	3.086	34.6
SSA 22a C30.....	8.2	16.4	24.67	0.53	>2.36	3.090	10.7
SSA 22a MD31.....	6.0	16.3	23.30	0.44	1.84	3.090	38.0
SSA 22a MD20.....	5.9	12.6	24.15	0.50	1.67	3.091	17.3
SSA 22a M9	4.9	15.1	24.75	0.83	>2.06	3.094	10.0
SSA 22a C5	2.6	9.6	23.64	0.78	>2.93	3.099	27.5
SSA 22a S1[d]	1.4	8.9	26.5:	...	...	3.100	...
SSA 22a C19.....	7.8	15.0	24.07	0.99	>2.53	3.103	18.6
SSA 22a C8	6.4	10.7	24.17	0.47	>2.96	3.108	17.0
SSA 22a C9	4.0	10.9	24.41	0.50	>2.82	3.108	13.7

[a] Using the coordinate system shown in Fig. 2.

[b] Defined by the position of the Lyα emission line.

[c] Star formation rate estimated from the UV continuum, assuming zero reddening, $\Omega_M = 0.2$, $\Omega_\Lambda = 0$, $H_0 = 70$ km s^{-1} Mpc^{-1}, and a Salpeter IMF evaluated from 0.1 $M_\odot$ to 100 $M_\odot$.

[d] Object found serendipitously; extremely faint in the continuum.

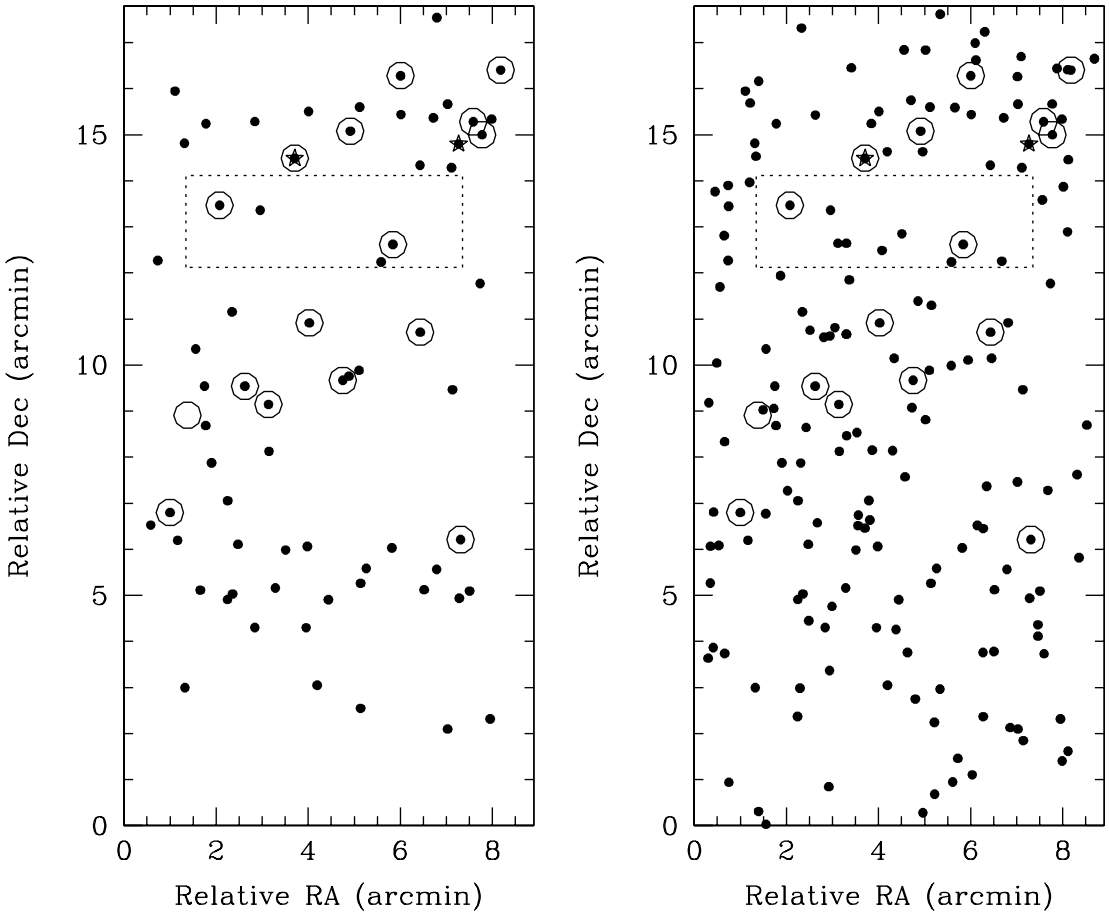

FIG. 2.—*Left panel*: Distribution on the plane of the sky of all Lyman-break objects with redshifts $z > 2$. The 16 objects with $\langle z \rangle = 3.090 \pm 0.02$ are circled (the object with a circle but no dot is SSA 22a S1, which was found serendipitously); the two QSOs are indicated by stars. *Right panel*: Same as the left-hand panel, but here the distribution of all color-selected (using the same criteria as for the spectroscopic sample on the left-hand panel) candidate $z \sim 3$ galaxies on the plane of the sky is shown. Again, objects known to be part of the structure at $z = 3.09$ are circled. The dotted region in both panels shows the approximate location and size of the SSA 22 Hawaii Deep Survey field (Cowie et al. 1996).

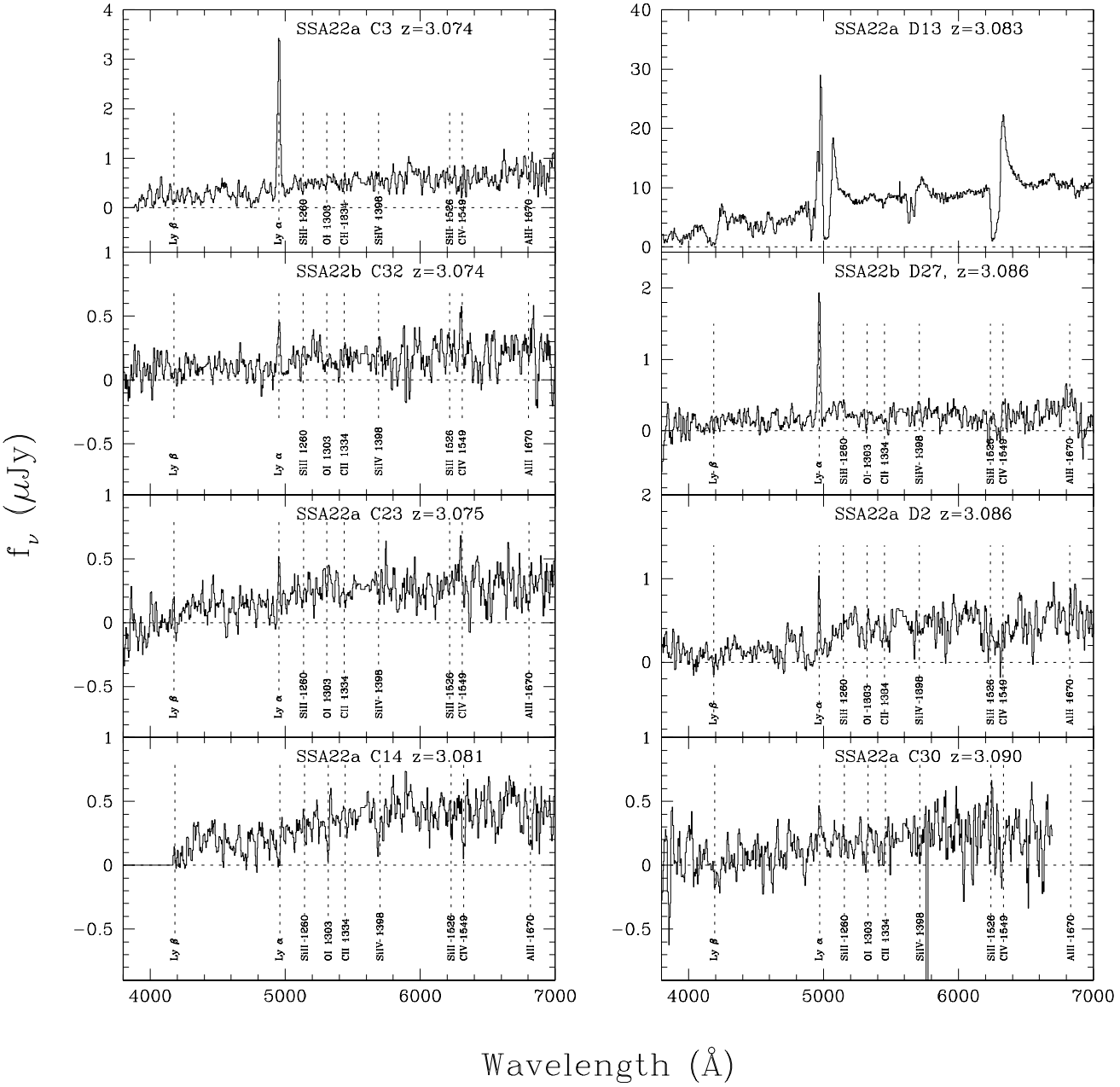

FIG. 3*a*

FIG. 3.—Spectra of the 16 objects in the redshift interval $3.07 \leq z \leq 3.11$. The positions of some of the features often seen in the spectra of high-redshift star-forming galaxies are indicated; not all of these features are evident in every spectrum. The absolute flux scale is only approximate; the photometry for each object is given in Table 1. The spectra have been smoothed by a kernel of width 12 Å (the spectral resolution) for display.

the desired redshift range, $2.7 \leq z \leq 3.4$. A total of 181 objects satisfy these adopted color criteria in the survey region, of which 113 satisfy the "robust" color criteria. Details of the selection criteria and of the resulting redshift selection function will be presented elsewhere (Steidel et al. 1998; Dickinson et al. 1998).

Approximately 80% of the objects assigned slits result in redshifts, with 78 objects having $z > 2$ and 59 having $2.7 \leq z \leq 3.4$. With the exception of a small amount of contamination by Galactic stars (approximately 5% of the objects satisfying the color criteria turn out to be Galactic stars, although there is essentially no contamination by stars for objects fainter than $\mathscr{R} = 24$), all identified color-selected objects are at high redshift ($z > 2$). Some of the spectra that remain unidentified may be objects at somewhat lower redshift than our primary selection window, since then the strongest spectral features would fall in regions of much lower instrumental sensitivity; however, there is no obvious trend with either $U_n - G$ color or apparent $\mathscr{R}$ magnitude for the unsuccessful redshifts. A higher success rate was achieved during 1996 October owing to much-improved photometry and (therefore) photometric selection, and also to higher quality slit masks. Nine of the objects with confirmed redshifts $z > 2$ (most having $2.0 \leq z \leq 2.5$) were subsequently shown not to satisfy either of the above selection categories on the basis of the improved photometry; in addition, two $z > 2$ objects were found serendipitously on slits designed for color-

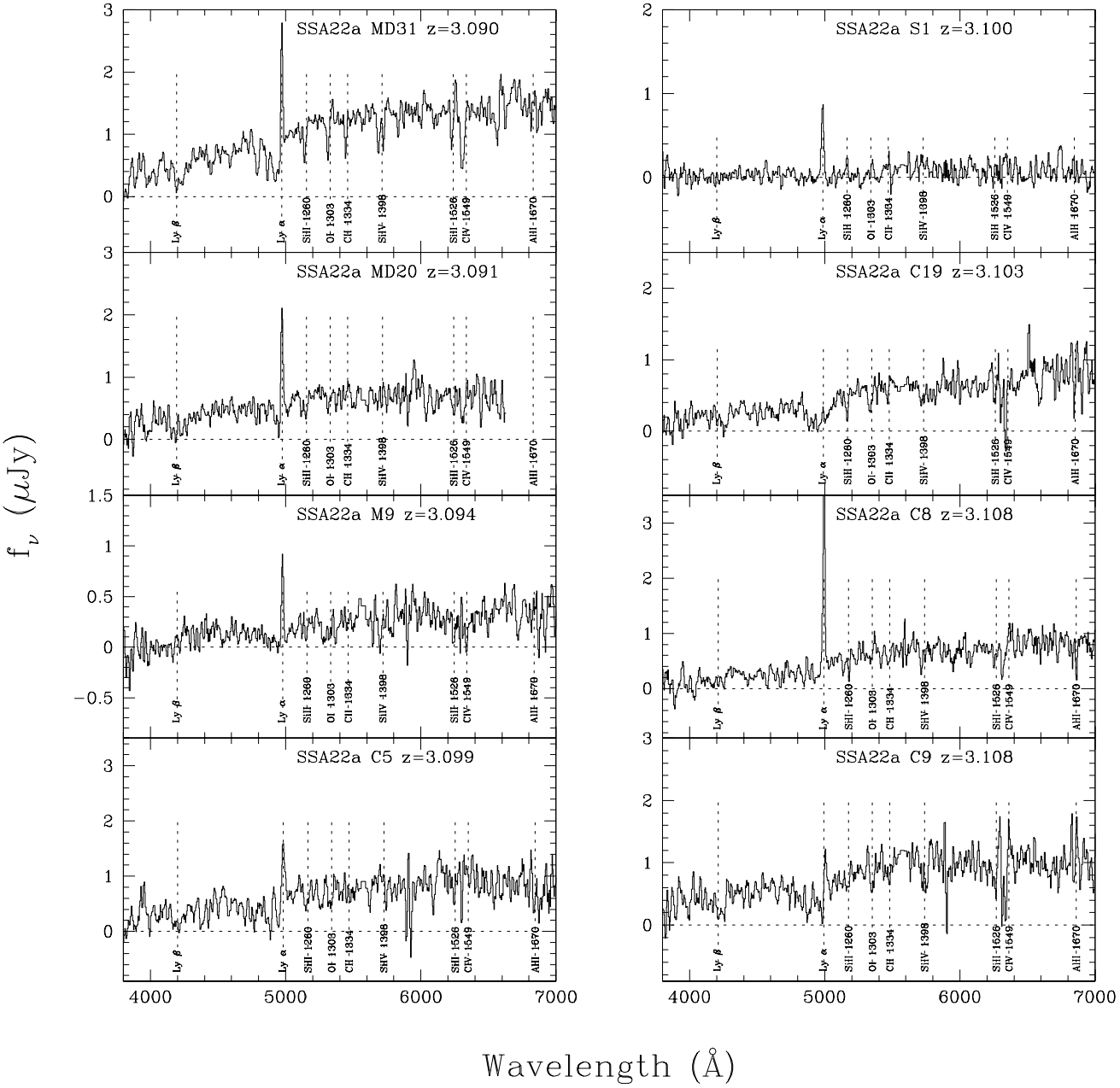

FIG. 3*b*

selected objects. For consistency, in the present paper we confine ourselves to only the 67 $z > 2$ objects satisfying the adopted photometric selection criteria given above, for which an accurate redshift selection function has been determined from the results of our spectroscopy in a number of different fields.

The redshifts of the galaxies in the sample were measured from strong absorption features in the rest-frame far-UV, mostly of interstellar origin (see Steidel et al. 1996b; Lowenthal et al. 1997) and, when present, the Lyα emission line. For spectra in which both absorption and emission are present, the redshifts defined by Lyα emission are systematically higher than the absorption-line redshifts by $\langle z_{\rm Ly\alpha} - z_{\rm abs} \rangle = 0.008 \pm 0.004$, or $\sim 600 \pm 300$ km s^{-1}. Based on limited near-IR spectroscopy of some of the high-redshift galaxies (Pettini et al. 1998), it appears that neither the emission lines nor the absorption lines actually coincide with the true systemic redshift of the galaxy; the "true" redshift probably lies between $z_{\rm abs}$ and $z_{\rm Ly\alpha}$. This uncertainty probably dominates over any measurement uncertainties, and so we adopt the standard deviation of the velocity difference as the typical uncertainty of the measured redshifts, $\sigma_v \approx 300$ km s^{-1}. Because most of the spectra exhibit Lyα emission at some level, whereas a smaller number of spectra exhibit only absorption features, we have adopted the position of Lyα emission as the primary redshift indicator.

A histogram of the $z > 2$ galaxies (and of the two faint QSOs that were discovered using the same photometric technique) in the SSA 22a + b field sample is given in Figure 1, with a bin size of $\Delta z = 0.04$, or $\Delta v \sim 3000$ km s^{-1} at $z \sim 3$. The distribution of the objects on the plane of the sky for both the spectroscopically confirmed and photometric candidate $z \sim 3$ samples is shown in Figure 2.

The most striking feature in the redshift histogram is the "spike" of 15 objects at $z \simeq 3.1$. In fact, one of the two $z > 2$ objects whose spectrum was obtained serendipitously also falls within the same redshift bin. The spectra of all 16 objects in this narrow redshift range are plotted in Figure 3, and the relative positions and photometry for the same objects are summarized in Table 1. We will not include the serendipitous object SSA 22a S1 in the analysis that follows, but it is intriguing that an object with strong Lyα emission (but very weak continuum emission) was found despite the very small effective solid angle covered by the mask slitlets.

3. IMPLICATIONS OF THE GALAXY OVERDENSITY

While spectroscopy in several fields suggests that our $U_n G\mathscr{R}$ selection criteria find galaxies over the broad range $2.7 \lesssim z \lesssim 3.4$ (Steidel et al. 1998), in this field, the one we have sampled most densely, nearly one-quarter of the redshifts lie between $z = 3.074$ and $z = 3.108$. A concentration this strong is unlikely to arise from Poisson sampling of our selection function—using the statistical technique described in the Appendix, we find that only one in 400 data sets generated by randomly drawing redshifts from our selection function (Fig. 1) contain as significant a departure from Poisson expectations—and so this group of galaxies almost certainly indicates a true peak in the density field at $z \sim 3.1$. From Figure 1, the approximate galaxy overdensity at this redshift is $\delta_{\rm gal} \sim 3.5$. At first glance this seems surprisingly large; in the local universe, the rms mass fluctuation in spheres of radius 8 h_{100}^{-1} Mpc is $\langle(\delta M/M)^2\rangle^{1/2} \equiv \sigma_8 \sim 0.6$, and since (for $\Omega_M = 1$) each bin in the histogram corresponds to a comoving volume of $\sim 8 \times 15 \times 15\, h_{100}^{-3}$ Mpc^3, we expect the relative mass fluctuation among bins $\sigma_{\rm mass}$ to be approximately $\sigma_8/(1+z) \simeq 0.15$. Yet the bin at $z \sim 3.1$ contains a galaxy overdensity $\delta_{\rm gal}$ that is 25 times larger than the expected $\sigma_{\rm mass}$. In this section, we will see what we can learn from the existence of this single large galaxy overdensity. The main conclusion will be the obvious one, that Lyman-break galaxies must be very biased tracers of mass. A more complete analysis of the galaxy distribution at $z \sim 3$ will be presented elsewhere.

Our approach will be straightforward. We will calculate a mass associated with the spike, treat the spike as a peak in the density field smoothed on this mass scale, and then calculate the probability of observing a peak so high within our survey volume for three representative cosmologies ($\Omega_M = 1$, $\Omega_M = 0.2$ open, and $\Omega_M = 0.3$ flat). The mass scale and peak height both depend on the bias parameter $b \equiv \delta_{\rm gal}/\delta_{\rm mass}$, and we will see how large the bias must be in order to make it reasonably probable that we would have observed the spike in our survey volume.

The first step is to calculate the mass associated with the spike. For concreteness we will consider only the 15 objects between $z = 3.074$ and $z = 3.108$ to be associated with the "spike" structure. This is the interval that maximizes the significance of the spike according to the statistical technique in the Appendix, and within it there is no evidence for substructure. A two-sample two-dimensional Kolmogorov-Smirnov test (Press et al. 1994) shows at the 95% level that galaxies in the spike have a different areal distribution from spectroscopically observed galaxies outside the spike, so the apparent "edge" of the spike in the southern half of the field (Fig. 2) is probably real. There is not much evidence, though, that we have observed an edge to the spike in any other direction, and thus we can only set a lower limit to its transverse size of $\sim 9' \times 11\farcm5$. For $\Omega_M = 1$, this corresponds to $\sim 11\, h_{70}^{-1}$ by $14\, h_{70}^{-1}$ comoving Mpc[2]. The effective depth of the structure for the same cosmology is $\sim 18\, h_{70}^{-1}/C$ comoving Mpc, where $C \equiv V_{\rm apparent}/V_{\rm true}$ takes into account the redshift space distortions caused by peculiar velocities. The mass associated with the structure is therefore $M = \bar{\rho} V(1+\delta_m) = 4.0 \times 10^{14}(1+\delta_m)/C\ h_{70}^{-1}\ M_\odot$,[7] where $\bar{\rho}$ is the mean density of the universe and δ_m, the mass overdensity, is related to the observed galaxy overdensity $\delta_{\rm gal,obs}$ through $1 + b\delta_m = C(1 + \delta_{\rm gal,obs})$. Following the prescription in the Appendix, we estimate a galaxy overdensity in this region of $\delta_{\rm gal,obs} = 3.6^{+1.4}_{-1.2}$.

It remains to estimate C. In principle, we do not even know if C is greater or less than one: a collapsing object will appear more dense in redshift space than in real space, while an object that has already collapsed and virialized will appear less dense in redshift space. We will see below, though, that it is difficult to produce even a moderately nonlinear overdensity on this mass scale at $z \simeq 3.1$, and so we will make the conservative assumption that we are observing an object that is just breaking away from the Hubble expansion rather than an object which has already collapsed. In this case, we can use the Zeldovich approximation to correct for peculiar velocities. In the Zeldovich approximation, each mass element maintains its linear-theory velocity, and, as a result, the density of a fluid element evolves according to $\rho/\bar{\rho} \equiv 1 + \delta_m = [(1 - D\lambda_1)(1 - D\lambda_2)(1 - D\lambda_3)]^{-1}$, where λ_i are initial eigenvalues of the tensor of deformation and $D(t)$ is the linear-growth factor. High peaks in the density field are roughly isotropic (Bardeen et al. 1986), and so we can reasonably use a simple expression for the redshift-distortion factor C (see, e.g., § 8 of Padmanabhan 1993) that holds when we view a collapsing object along a principal axis:

$$C = \frac{1 - D(1+f)\lambda_3}{1 - D\lambda_3}\,,$$

where $f \equiv d\ln D/d\ln a \simeq \Omega_M^{4/7}(z)$ (Lahav et al. 1991). For $\lambda_1 = \lambda_2 = \lambda_3$, this becomes $C = 1 + f - f(1+\delta_m)^{1/3}$, which is the expression we use.

After we have estimated the peak height ν (defined below), we can return to this peculiar-velocity correction and gauge how wrong our assumption of isotropy is likely to have been. In the high-peak limit, the eigenvalues of the deformation tensor have approximate relative sizes $\lambda_1 : \lambda_2 : \lambda_3 \sim 1 + 1.5/\nu : 1 : 1 - 1.5/\nu$ (Bond 1988). We will see below that ν ranges from 2 to 5 for the parameter values we consider (Table 2), and so the assumption of isotropy is poor in some cases. Fortunately, the peculiar-velocity correction is smallest when the assumption is worst, and in the end our conclusions would not be affected much by the expected level of anisotropy. We make a crude attempt to quantify this by randomly rotating a deformation tensor with eigen-

[7] We note that this mass scale is 1–2 orders of magnitude larger than the minimum mass scale that would be derived for typical "spikes" in lower redshift pencil-beam surveys such as those in Cohen et al. (1996a, 1996b). The main difference is that working with a relatively large field at $z \sim 3$ provides a much larger comoving field of view, and so we are able to set a correspondingly larger lower limit to the size of structures we observe. Given our much sparser sampling density, we are probably sensitive only to structures on relatively large angular scales; because the relevant mass scales are (potentially) so different, the relationship between this structure and those seen in other pencil-beam surveys is not at all clear.

TABLE 2

SUMMARY OF STATISTICS FOR DIFFERENT COSMOLOGICAL MODELS

MODEL PARAMETERS	$\Omega_M = 1$			$\Omega_M = 0.2$			$\Omega_M = 0.3$, $\Omega_\Lambda = 0.7$		
	$b = 4$	$b = 6$	$b = 8$	$b = 1$	$b = 1.5$	$b = 2$	$b = 2$	$b = 3$	$b = 4$
$M_{\rm halo}$ [a]	0.9	3	6	0.04	0.6	2	0.1	0.8	2
$M_{\rm spike}$ [b]	8.2	6.9	6.2	14	11	8.9	14	11	9.8
$\delta_{\rm mass}$ [c]	0.68	0.49	0.38	2.2	1.6	1.3	1.1	0.86	0.68
$\delta_{{\rm mass},L}$ [d]	0.44	0.35	0.29	0.80	0.71	0.64	0.60	0.51	0.44
$\nu_{\rm Gauss}$ [e]	4.9	3.7	3.0	3.2	2.7	2.3	4.3	3.4	2.8
$\nu_{\rm STH}$ [f]	3.6	2.7	2.1	2.6	2.2	1.9	3.3	2.6	2.2
$N_{\rm pk}$ [g]	10^{-4}	0.03	0.20	0.02	0.09	0.22	0.001	0.03	0.14
$N_{\rm STH}$ [h]	0.003	0.07	0.33	0.03	0.14	0.35	0.006	0.07	0.23

[a] Mass of the dark halos that harbor individual Lyman-break galaxies, derived from the bias assuming the $n = 1, h_{70} = 1$ CDM spectrum discussed in the text. Units of $10^{12}\ M_\odot$.

[b] Mass scale of "spike" structure, in units of $10^{14}\ M_\odot$.

[c] True mass overdensity associated with spike.

[d] Linear mass overdensity associated with spike.

[e] $\delta_{{\rm mass},L}/\sigma_{\rm Gauss}$, where $\sigma_{\rm Gauss}$ is the rms relative mass fluctuation in the density field smoothed by a Gaussian on mass scale M.

[f] $\delta_{{\rm mass},L}/\sigma_{\rm STH}$, where $\sigma_{\rm STH}$ is the rms relative mass fluctuation in the density field smoothed by a spherical top hat on mass scale M.

[g] Expected number of peaks of height $\delta_{{\rm mass},L}$ in Gaussian-smoothed density field, per surveyed volume. From Bardeen et al. 1986.

[h] Alternate estimate of expected peak number density.

values in the "typical" ratio above and calculating the exact peculiar-velocity correction for each rotation. Even in the worst case ($\nu \sim 2$), the 1 σ spread in C is only about 10% across the randomly rotated ensemble. This is small compared to the Poisson uncertainty in $\delta_{\rm gal,obs}$ and will be neglected.

We can now calculate $M_{\rm spike}$ and δ_m for any assumed bias. Selected values are shown in Table 2. The final step is to calculate whether the density field smoothed on mass scale $M_{\rm spike}$ would plausibly contain a peak of height δ_m in our survey volume. This will let us assess whether an assumed bias value is consistent with the existence of the spike. Because rms fluctuations on the (large) mass scale $M_{\rm spike}$ are much smaller than unity, the smoothed density field should be well approximated by linearly evolved initial conditions, and we should be able to use linear theory to calculate the probability of observing a peak of height δ_m. The one complication is that nonlinear effects may have begun to accelerate the peak's growth; in order to analyze the spike with linear theory, we will need to estimate the linear theory height δ_L that corresponds to the measured peak height δ_m. Spherically symmetric collapse is one of the few cases where nonlinear growth is quantitatively understood, and it would be convenient if we could use spherical collapse results to correct for nonlinear growth in our spike. But how accurately can we model the growth of a peak through spherical collapse? One issue is whether the peak is likely to have been roughly spherical in the first place, and we saw above that this is strongly affected by its height $\nu \equiv \delta_L/\sigma$, where σ is the rms relative mass fluctuation on the mass scale of the spike. A second issue is whether the previous collapse of smaller perturbations within the peak could generate nonradial motions large enough to slow down—or prevent—the peak's collapse (see, e.g., Peebles 1990). This depends on the spectral index of density fluctuations n, where $|\delta_k|^2 = Ak^n$, because (for fixed A) n controls the level of small-scale power. Bernardeau (1994) argues that for $\nu \gtrsim 2$ and $n < -1$ typical peaks will grow at roughly the rate predicted by the spherical collapse model, at least until $\delta_m \simeq 4$, and this conclusion is supported by the N-body experiment of Thomas & Couchman (1992). Since in all scenarios considered, the spike overdensity satisfies $\nu \gtrsim 2$, and since cold dark matter (CDM) spectra on the mass scales of interest to us have effective spectral indices $n_{\rm eff} \lesssim -1$, we will adopt the spherical collapse $\delta_m \rightarrow \delta_L$ transformation as approximated by Bernardeau (1994), $\delta_L = 1.5[1 - (1 + \delta_m)^{-2/3}]$. This should at least give us a lower limit on δ_L, since previous collapse on smaller scales (which we have neglected) slows down nonlinear growth.

Table 2 shows two estimates of the number density of regions with mass overdensity $\geq \delta_L$ for each cosmology and bias value. The first estimate, $N_{\rm Gauss}$, is the number density $n_{\rm pk}(> \delta_L)$ of peaks of height $\geq \delta_L$ in the Gaussian-smoothed density field, from Bardeen et al. (1986; hereafter BBKS). For the second estimate we use the traditional

$$N_{\rm STH} = \frac{\bar{\rho}}{2M_{\rm spike}}\left[1 - {\rm erf}\left(\frac{\delta_L}{\sqrt{2}\sigma_{\rm STH}}\right)\right],$$

where $\sigma_{\rm STH}$ is the rms relative mass fluctuation in the density field smoothed by a spherical top hat on mass scale $M_{\rm spike}$. Both $N_{\rm Gauss}$ and $N_{\rm STH}$ have been normalized to units of 1 over our survey volume, which we will take to be an 18′ by 9′ rectangular field between $z = 2.7$ and $z = 3.4$. If $N \sim 1$ in this table, then we would expect to see, on average, one peak with linear height $> \delta_L$ in a volume this size, and the corresponding bias value and cosmology are roughly consistent with the existence of the spike. $N_{\rm Gauss}$ ($\equiv n_{\rm pk}$) is also presented in graphical form in Figure 4 to give an idea of the uncertainties involved. $N_{\rm Gauss}$ and $N_{\rm STH}$ were calculated assuming a Harrison-Zeldovich ($n = 1$) primordial spectrum modified by the BBKS adiabatic CDM transfer function with $q = k/\Gamma h$ (Γ is a spectral shape parameter that we will discuss more below) and normalized so that

$$\sigma(r_0 = 8\ h_{100}^{-1}\ {\rm Mpc}) = \frac{\sigma_8}{1 + z}\,\frac{g[\Omega_M(z), \Omega_\Lambda(z)]}{g[\Omega_M(0), \Omega_\Lambda(0)]},$$

where $g(\Omega_M, \Omega_\Lambda)$ is the linear growth suppression factor from Carroll, Press, & Turner (1992) and σ_8, the $z = 0$ cluster normalization, is from Eke, Cole, & Frenk (1996).

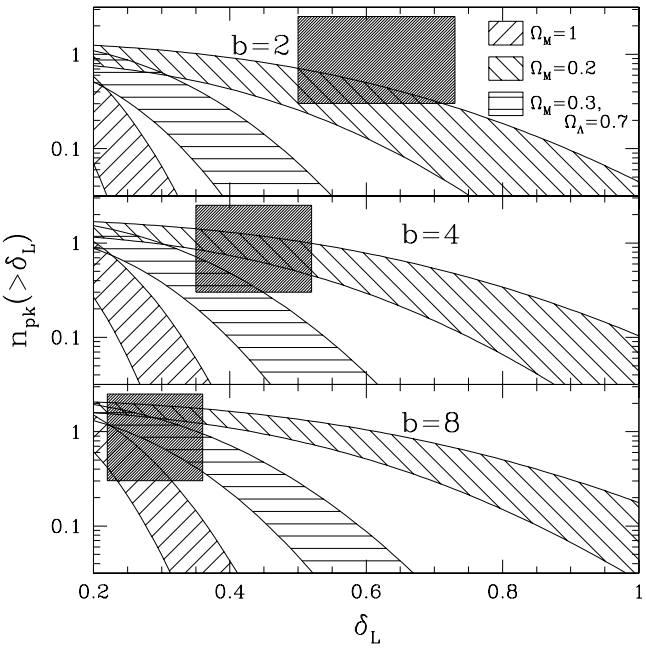

FIG. 4.—Reconciling the observed galaxy overdensity with various cosmological scenarios. The smooth curves show the expected number of peaks in this field with linear overdensity greater than δ_L. The shaded boxes show the approximate peak height and number density deduced from our observations. The actual box position is slightly different for each of the cosmologies, but this difference is insignificant for our purposes. If a curve passes through the box, then the corresponding parameter values are at least roughly consistent with the existence of the spike in the redshift histogram. The x range of the box is a 68% confidence interval that takes into account only the (Poisson) uncertainties in δ_{gal}; the y range of the box $0.3 < n_{pk} < 2.5$ is also an approximately 68% interval on the number density of similar structures at $z \sim 3$, based on the fact that we have detected one such overdensity in the first densely sampled field. The two smooth curves for each cosmology give an idea of the uncertainty in n_{pk}. The upper curve applies if the true mass of the structure is 1 σ lower than our best estimate and the normalization σ_8 is 1 σ higher than the best estimate of Eke, Cole, & Frenk (1996). The lower curve applies if the mass of the structure is 1 σ higher and the normalization is 1 σ lower than the best estimates. See text.

We adopt cluster normalization because it is on the same length scale as our structure; *COBE* measurements are on a considerably larger scale, and uncertainties in the spectral tilt n make *COBE* measurements less constraining. Since the normalization we have adopted is determined on roughly the same scale as the spike, our conclusions will be insensitive to the shape of the power spectrum. In making Table 2 and Figure 4, we used the CDM shape parameter from Sugiyama (1995), $\Gamma \simeq \Omega_M\ h_{100} \exp(-\Omega_B - \Omega_B/\Omega_M)$ with $h_{100} = 0.7$ and $\Omega_B = 0.024/h_{100}^2$ (Tytler, Fan, & Burles 1996), but our conclusions about b would not change significantly for any value of Γ in the range $0.1 < \Gamma < 0.7$.

It is clear from Table 2 and Figure 4 that an overdensity similar to the one we observe would not occur in any of these cosmologies unless Lyman-break galaxies were very biased tracers of mass. The minimum bias values for $\Omega_M = 1$, $\Omega_M = 0.2$ open, and $\Omega_M = 0.3$ flat are approximately 6, 2, and 4, respectively. These high values have interesting implications. In the biasing model of Mo & White (1996), the mass of a dark halo M can be (implicitly) estimated from its bias b and redshift z through

$$\sigma(M, z) = \frac{\delta_c}{\sqrt{(b-1)\delta_c + 1}},$$

where $\sigma(M, z)$ is the rms relative mass fluctuation on scale M at redshift z, and $\delta_c \sim 1.7$. Because σ is a decreasing function of M, heavier halos are more highly biased. From Table 2, the large bias values required to explain the spike imply Lyman-break halo masses of a few times $10^{12}\ M_\odot$ in each cosmology considered. The exact halo mass that corresponds to a given bias is spectrum dependent and can change by a factor of a few for choices of Γ different from the h_{70} Sugiyama (1995) value we have used.

In summary, then, we started out with a galaxy overdensity that naively seemed ~ 25 times larger than the expected σ_{mass}. We argued that part of this factor of 25 could be accounted for through peculiar velocities, part through nonlinear effects and part through the suppression of linear growth in cosmologies with $\Omega_M < 1$. However, we were still left with a galaxy overdensity several times larger than the expected σ_{mass}, and we concluded that Lyman-break galaxies are very biased tracers of mass. A large bias is not unexpected, provided that these galaxies are massive systems. The existence of the spike lends further support to a halo mass scale of $\sim 10^{12}\ M_\odot$ for these galaxies.

4. CORRELATION OF PEAKS WITH QSO ABSORPTION FEATURES

Two of the objects in the spectroscopic sample are high redshift QSOs. One of them, called SSA 22a D13, has $z_{em} = 3.083$ ($\mathscr{R} = 21.7$) and thus is part of the prominent redshift "spike" at $\langle z \rangle = 3.090$, discussed at length in § 3. A second QSO, called SSA 22a D14, has $z_{em} = 3.356$ and $\mathscr{R} = 20.8$, and even at the coarse resolution (~ 12 Å) of our survey spectra, several metal-line absorption systems are evident (see Fig. 5). There is a probable damped Lyα system at $z_{abs} = 2.937$, an optically thick Lyman-limit system at $z_{abs} = 3.288$, another metal-line system having a relatively strong Lyα absorption line, and the C IV $\lambda\lambda$1548, 1550 doublet at $z_{abs} = 3.094$. We note that these coincide with the three strongest peaks in the redshift histogram (although, as discussed above, only the one at $z = 3.09$ is formally of high statistical significance). We also note that there is no confirmed Lyman-break galaxy or photometrically selected candidate that is near enough to the sightline of SSA 22a D14 to be (plausibly) responsible for any of these absorption systems, adding to the growing number of high redshift absorption systems that are fainter than our typical limits for the detection of Lyman-break galaxies, $\mathscr{R} = 25.5$ (see Steidel et al. 1995). It would clearly be of great interest to obtain a higher resolution spectrum of SSA 22a D14 so that the nature of the absorption-line systems could be better discerned.

There are two additional metal-line systems with relatively strong C IV doublets but weaker Lyα lines at $z_{abs} = 2.740$ and 2.801. There are no obvious features at these redshifts in the galaxy redshift histogram, but these redshifts are near the tail of our selection function, and so the volume is not well sampled using our current color criteria.

The fortuitous placement of two reasonably bright QSOs within the SSA 22 field is obviously of great interest for a comparison of the structure seen in emission versus that seen in absorption along the same line of sight. Although the significance is not completely clear, the fact that all three of the most prominent features in the redshift histogram have counterparts in metal-line absorption systems is particularly intriguing (see Francis et al. 1996) and suggestive of

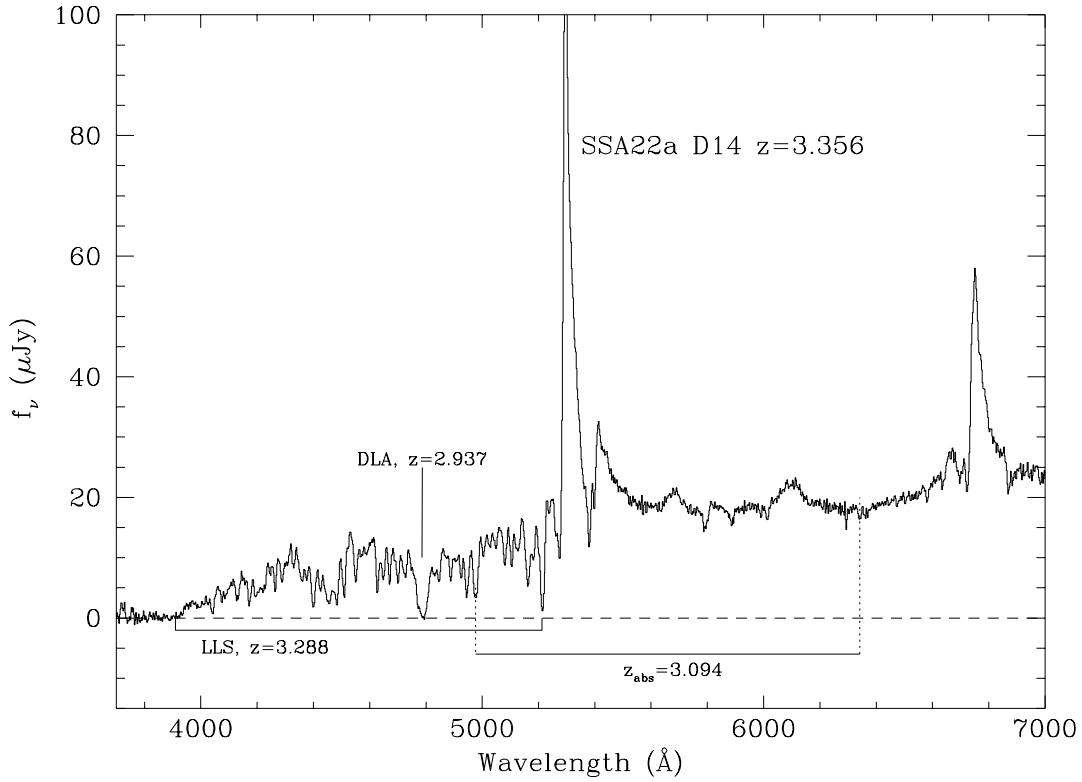

FIG. 5.—Spectrum of QSO SSA 22a D14, with the metal-line absorption systems corresponding to the redshifts of the three most significant features in the SSA 22a + b redshift histogram marked (see text).

large-scale coherence (with a large covering fraction) in the overall distribution of gas and stars at high redshift. While suggestions of large-scale structure in absorbing gas from correlations of QSO absorption-line systems (both transverse to and along the line of sight) have been many (see, e.g., Jakobsen et al. 1986; Sargent & Steidel 1987; Steidel & Sargent 1992; Dinshaw & Impey 1996; Williger et al. 1996; Quashnock, Vandenberk, & York 1996), it is now possible to compile large samples of high-redshift galaxies at the same redshifts, and there is clearly a great deal of very fruitful work to be done in combining the absorption and emission techniques to obtain as complete a picture as possible of the distribution of baryons at these early epochs.

5. SUMMARY

We have presented evidence for a large structure of galaxies at $z \simeq 3.1$ on the basis of a pronounced "overdensity" in a redshift histogram of photometrically selected field galaxies, coupled with the distribution of the galaxies within this redshift-space "spike" on the plane of the sky. A relatively simple analysis of this structure (§ 3) shows that these early star-forming galaxies must be very biased tracers of mass, with a higher bias ($b \gtrsim 6$) required in standard $\Omega_M = 1$ CDM than in $\Omega_M = 0.2$ open CDM ($b \gtrsim 2$) or in $\Omega_M = 0.3$ Λ-CDM ($b \gtrsim 4$). A large bias is expected for massive galaxies, and a major conclusion of this paper is that these Lyman-break galaxies are indeed massive systems ($M \sim 10^{12}\ M_\odot$), as we originally claimed on different grounds (Steidel et al. 1996b). A similarly large mass for these galaxies was also predicted by Baugh et al. (1998) on the basis of simple assumptions about star and dark-halo formation, and it is encouraging that independent estimates of these galaxies' masses should agree so well.

An interesting sidelight is that the volume of one of our survey fields (a few $\times 10^5$ Mpc^3) is well matched to the present-day density of X-ray–selected clusters with $kT \gtrsim 2.5$ keV ($\sim 3 \times 10^{-6}\ h_{70}^3$ Mpc^{-3}; Eke et al. 1996). In an average field of this volume, we would expect to see 0.3, 1.0, 1.1 structure that is destined to become a cluster by the present day for $\Omega_M = 1$, $\Omega_M = 0.2$ open, and $\Omega_M = 0.3$ flat, and this raises the possibility that structure we have found at $z \sim 3.1$ may be an Abell cluster in its infancy. It is on the right mass scale, and (depending on the bias) its linear overdensity δ_L when evolved to the present day could reach the spherical top-hat threshold of $\delta_L \simeq 1.7$ for collapse and virialization. Given the sampling density of the photometrically selected candidates in the SSA 22a + b field, we have probably only found $\sim$30%–50% of the objects in the $\langle z \rangle = 3.09$ structure to the same apparent magnitude level. If each Lyman-break galaxy is the progenitor of a present-day galaxy brighter than L^*, this would imply $\sim$30–50 such galaxies within the structure, lending further support to the notion that the "spike" is a protocluster. In many respects, the structure we have identified is very similar to a less evolved version of the structure found at $z = 0.985$ by Le Fèvre et al. (1994) as part of the Canada-France Redshift Survey.

The results we have presented above are based on a single field of a "targeted" redshift survey using Lyman-break photometric selection criteria and focusing on the redshift range $2.7 \lesssim z \lesssim 3.4$. A larger sample will test the validity of the conclusions outlined here and will give a full picture of the correlation function of star-forming galaxies at high redshift on scales from kpc to tens of Mpc. Whether or not one can reach significant cosmological conclusions on the basis of only about 70 redshifts in one field, we regard it as

extremely promising that one can now feasibly observe the large-scale distribution of galaxies at very early epochs. We would also like to emphasize how efficiently one can address these issues by using photometric methods to "preselect" the volume/epoch studied. Lyman-break galaxies at $z \sim 3$ are merely one example.

We would like to thank the staff of both the Palomar and Keck Observatories, as well as the entire team of people responsible for the Low Resolution Imaging Spectrograph, led by J. B. Oke and J. Cohen, for making these observations possible. We would also like to thank A. Phillips for allowing us to use his slitmask alignment software. We benefited from several useful conversations with T. Padmanabhan and J. Peacock. S. D. M. White's detailed comments on an earlier draft improved the clarity of § 3. We are grateful to the referee, D. Koo, for constructive comments. C. C. S. acknowledges support from the National Science Foundation through grant AST 94-57446 and from the Alfred P. Sloan Foundation. M. G. has been supported through grant HF-01071.01-94A from the Space Telescope Science Institute, which is operated by the Association of Universities for Research in Astronomy, Inc., under NASA contract NAS 5-26555.

APPENDIX

STATISTICAL SIGNIFICANCE OF FEATURES IN THE REDSHIFT DISTRIBUTION

We use a simple method to look for clustering in the galaxy redshifts. Rather than placing the redshifts into bins and looking for unusually crowded bins (see, e.g., Cohen et al. 1996b), we scan our unbinned data for galaxy pairs, triplets, quartets, and so on whose redshifts are closer together than we would expect from Poisson statistics. If the product of our selection function and the density of Lyman-break galaxies were equal to a known constant λ over the redshift range of interest, then without clustering the probability that a group of N galaxies would span a redshift interval Δz would be given by the Erlangian distribution (Eadie et al. 1971)

$$p(\Delta z \,|\, N\lambda) = \lambda(\lambda\,\Delta z)^{N-2} \exp(-\lambda\,\Delta z)/(N-2)! \; .$$

In this case, it would be easy to find significantly clustered groups of galaxies; we could simply consider each group of N neighboring galaxies in turn and calculate the probability that, in the absence of clustering, they would be contained in a redshift interval smaller than the observed Δz_0,

$$p(\Delta z < \Delta z_0) = \int_0^{\Delta z_0} p(\Delta z \,|\, N\lambda) d(\Delta z) = \frac{\gamma(N-1,\, \Delta z_0)}{\Gamma(N-1)} \, ,$$

with γ, the (unnormalized) incomplete gamma function, given, e.g., in Press et al. (1994). If this probability were very close to zero, it would suggest that the small separation of the N neighbors was inconsistent with Poisson sampling of a uniform background, and we would consider those N galaxies a cluster candidate. (In this section we use "cluster" to denote an arbitrarily small—or large—group of galaxies whose proximity is unexpected from Poisson statistics.)

In practice, the product λ of our selection function and the mean density of Lyman-break galaxies is neither precisely known nor constant with redshift, and so we proceed as follows. First, we estimate the shape of $\lambda(z)$ by placing the redshifts of all our spectroscopically confirmed marginal and robust Lyman-break galaxies (there are 208, of which 69 are in SSA 22a or SSA 22b) into bins of width $\Delta z = 0.2$ and fitting the resulting histogram with a cubic spline (see Fig. 1). We then transform our redshifts z into a coordinate system t in which λ is roughly constant, and the problem is reduced to searching for significantly clustered groups of galaxies in the midst of a constant Poisson background of unknown intensity λ.

This is just the "on-source/off-source" problem familiar from high-energy astrophysics, where we observe N_1 counts during a time interval t_1 in one part of the sky and N_2 during t_2 in another and must decide whether there is any evidence for an intrinsically higher count rate in the second region. In our case, we want to decide whether there is evidence for the presence of a cluster (i.e., an elevated count rate) in the redshift interval t_2 between two arbitrarily selected galaxies. We begin by estimating the "background count rate" λ from the density of galaxies outside this candidate cluster. If there are N_1 galaxies at redshifts less than or equal to the cluster member with the lowest redshift and N_3 galaxies at redshifts greater than or equal to the cluster member with the highest redshift, Bayes's Theorem gives

$$p(\lambda \,|\, t_1\, t_3\, N_1\, N_3) = \frac{p(t_1\, t_3 \,|\, \lambda N_1\, N_3) p(\lambda \,|\, N_1\, N_3)}{\int d\lambda' p(t_1\, t_3 \,|\, \lambda' N_1\, N_3) p(\lambda' \,|\, N_1\, N_3)} \, ,$$

where t_1 is the interval between the galaxy in our sample with the lowest redshift and the cluster member with the lowest redshift, and t_3 is the interval between the cluster member with the highest redshift and the galaxy in our sample with the highest redshift. With this probabilistic distribution for λ, we can proceed analogously to the case above where λ was known exactly. Since the probability that the group of N_2 galaxies would be contained in exactly the observed interval t_2 is

$$p(t_2 \,|\, N_1\, N_2\, N_3\, t_1\, t_3) = \int d\lambda p(t_2 \,|\, \lambda N_1\, N_2\, N_3\, t_1\, t_3) p(\lambda \,|\, N_1\, N_2\, N_3\, t_1\, t_3) \, ,$$

the probability that they would be contained in an interval smaller than the observed t_2 is

$$p(t < t_2) = I_x(N_1 + N_3 - 1,\, N_2 - 1) \equiv \zeta \, ,$$

where $x \equiv (t_1 + t_3)/(t_1 + t_2 + t_3)$, I_x is the incomplete beta function (Press et al. 1994), and we have substituted the Erlangian distribution for $p(t \mid N\lambda)$, assumed a uniform prior for λ over the interval $(0, \lambda_{\max})$, and taken the limit $\lambda_{\max} \to \infty$ (for more detailed derivations of similar results, see Jaynes 1990; Loredo 1992). This expression for ζ lets us assess the degree to which the redshifts of any N_2 adjacent galaxies are inconsistent with Poisson sampling of a uniform background; groups of galaxies with ζ very close to 0 (or to 1) are not expected in the absence of clustering, and so by calculating ζ for all groups of N_2 adjacent galaxies in our sample, with $N_2 = 2, 3, 4, \ldots$, we can locate the most statistically significant clusters (or voids) in our redshift distribution. In practice, we restrict our attention to clusters (or voids) with $\Delta z \leq 0.2$, since larger features are interpreted with this technique as parts of the selection function rather than as parts of of the galaxy distribution.

After using this procedure to locate candidate clusters in our redshift distribution, we estimate the significance of each cluster by comparing its ζ to the distribution of ζ in simulated data sets with redshifts randomly drawn from the smooth selection function in Figure 1. If a candidate cluster has a ζ so small that it appears in only one of 100 random data sets, we assign that cluster a significance of 99%.

This technique has the obvious flaws that the estimate of the background level is not correct when there is more than one strong spike in the data and that we take no account of correlations between galaxies in calculating significances. Neither is critical in the present application because we have only one dominant spike and it is on a scale many times larger than the Lyman-break galaxy correlation length (Giavalisco et al. 1998).

Once we have identified a significant cluster, we may want to associate an overdensity δ with it though the relationship $\delta \equiv n_{\rm cluster}/\bar{n} - 1$, where $n_{\rm cluster}$ is the number density of galaxies within the cluster and $\bar{n}$ is the background number density. $\bar{n}$ will in general be well determined by the many galaxies outside the cluster, but $n_{\rm cluster}$ is more problematic. We are defining the edge of the cluster to fall exactly on the members with the lowest and highest redshifts, so should we include those two galaxies in estimating $n_{\rm cluster}$? In § 3, we exclude from the $n_{\rm cluster}$ calculation any galaxy whose position is explicitly used in defining the cluster boundary. There are three such galaxies—one sets the low-redshift edge, another the high-redshift edge, and the third sets the southern edge of the cluster (Fig. 2). To estimate $n_{\rm cluster}$, we use the formula

$$p(n \mid NV) = V \frac{(nV)^{N-3} e^{-nV}}{(N-3)!},$$

with $N = 15$.

REFERENCES

Bardeen, J. M., Bond, J. R., Kaiser, N., & Szalay, A. S. 1986, ApJ, 304, 15
Baugh, C. M., Cole, S., Frenk, C. S., & Lacey, C. G. 1998, ApJ, submitted
Bernardeau, F. 1994, ApJ, 427, 51
Bond, J. R. 1988, in Large-Scale Motions in the Universe: A Vatican Study Week, ed. V. C. Rubin & G. V. Coyne (Princeton: Princeton University Press), 419
Brainerd, T. G., Smail, I., & Mould, J. R. 1995, MNRAS, 275, 781
Brainerd, T. G., & Villumsen, J. V. 1992, ApJ, 400, 398
Broadhurst, T., Ellis, R., Koo, D., & Szalay, A. 1990, Nature, 343, 726
Carlberg, R. G., Cowie, L. L., Songaila, A., & Hu, E. 1997, ApJ, 484, 538
Carroll, S. M., Press, W. H., & Turner, E. L. 1992, ARA&A, 30, 499
Cohen, J. G., Cowie, L. L., Hogg, D. W., Songaila, A., Blandford, R., Hu, E., & Shopbell, P. 1996a, ApJ, 471, L5
Cohen, J. G., Hogg, D. W., Pahre, M. A., & Blandford, R. 1996b, ApJ, 462, L9
Cole, S., & Kaiser, N. 1989, MNRAS 237, 1127
Connolly, A. J., Szalay, A. S., Koo, D. C., Romer, A. K., Holden, B., Nichol, R. C., & Miyaji, T. 1996, ApJ, 473, L67
Cowie, L. L., Songaila, A., Hu, E. M., & Cohen, J. G. 1996, AJ, 112, 839
de Lapparent, V., Geller, M. J., & Huchra, J. P. 1986, ApJ, 302, L1
Dickinson, M., et al. 1998, in preparation
Dinshaw, N., & Impey, C. D. 1996, ApJ, 458, 73
Eadie, W. T., Drijard, D., James, F. E., Roos, M., & Sadoulet, B. 1971, Statistical Methods in Experimental Physics (Amsterdam: North-Holland)
Efstathiou, G. 1995, MNRAS, 272, 25
Eke, V. R., Cole, S., & Frenk, C. S. 1996, MNRAS, 282, 263
Francis, P. J., et al. 1996, ApJ, 457, 490
Giavalisco, M., Steidel, C. C., Adelberger, K., Dickinson, M., & Pettini, M. 1998, in preparation
Giavalisco, M., Steidel, C. C., & Machetto, F. 1996, ApJ, 470, 189
Jakobsen, P., Perryman, M. A., Ulrich, M. H., Machetto, F., & Di Serego-Alighieri, S. 1986, ApJ, 303, L27
Jaynes, E. T. 1990, in Maximum Entropy and Bayesian Methods, ed. P. F. Fougère (Dordrecht: Kluwer), 1
Kaiser, N., & Peacock, J. A. 1991, ApJ, 379, 482
Lahav, O., Lilje, P. B., Primack, J. R., & Rees, M. J. 1991, MNRAS, 251, 128
Landy, S. D., Shectman, S. A., Lin, H., Kirshner, R. P., Oemler, A., & Tucker, D. L. 1996, ApJ, 456, L1
Le Fèvre, O., Crampton, D., Hammer, F., Lilly, S. J., & Tresse, L. 1994, ApJ, 423, L89
Le Fèvre, O., Hudon, D., Lilly, S. J., Crampton, D., Hammer, F., & Tresse, L. 1996, ApJ, 461, 534
Lilly, S. J., Le Fèvre, O., Crampton, D., Hammer, F., & Tresse, L. 1995, ApJ, 455, 50
Loredo, T. J. 1992, in Statistical Challenges in Modern Astronomy, ed. E. Feigelson & G. J. Babu (New York: Springer), 275
Lowenthal, J. D., et al. 1997, ApJ, 481, 673
Mo, H. J., & Fukugita, M. 1996, ApJ, 467, L9
Mo, H. J., & White, S. D. M. 1996, MNRAS, 282, 347
Oke, J. B., et al. 1995, PASP 107, 3750
Padmanabhan, T. 1993, Structure Formation in the Universe (Cambridge: Cambridge Univ. Press)
Peebles, P. J. E. 1990, ApJ, 365, 27
Pettini, M., Steidel, C. C., Dickinson, M., Kellogg, M., Giavalisco, M., & Adelberger, K. L. 1998, in AIP Conf. Proc. The Ultraviolet Universe at Low and High Redshift, ed. W. Waller (New York: AIP), in press
Press, W. H., Teukolsky, S. A., Vetterling, W. T., & Flannery, B. P. 1994, Numerical Recipes in C (2d ed.; New York: Cambridge Univ. Press)
Quashnock, J. M., Vandenberk, D. E., & York, D. G. 1996, ApJ, 472, L69
Sargent, W. L. W., & Steidel, C. C. 1987, ApJ, 322, 142
Shectman, S. A., et al. 1996, ApJ, 470, 172
Steidel, C. C., Giavalisco, M., Dickinson, M., & Adelberger, K. L. 1996a, AJ, 112, 352
Steidel, C. C., Giavalisco, M., Pettini, M., Dickinson, M., & Adelberger, K. L. 1996b, ApJ, 462, L17
Steidel, C. C., & Hamilton, D. 1993, AJ, 105, 2017
Steidel, C. C., Pettini, M., & Hamilton, D. 1995, AJ, 110, 2519
Steidel, C. C., & Sargent, W. L. W. 1992, ApJS, 80, 1
Steidel, C. C., et al. 1998, in preparation
Sugiyama, N. 1995, ApJS, 100, 281
Thomas, P. A., & Couchman, H. M. P. 1992, MNRAS, 257, 11
Tytler, D., Fan, X.-M., & Burles, S. 1996, Nature, 381, 207
White, S. D. M. 1997, in The Early Universe with the VLT, ed. J. Bergeron (Berlin: Springer), 219
Williger, G. M., Hazard, C., Baldwin, J. A., & McMahon, R. G. 1996, ApJS, 104, 45